nanomanufacturing

MDPI

Article

Lipid–Inorganic Hybrid Particles with Non-Lamellar Structures

Benjamin Schmidbauer, Frank Uhlig and Angela Chemelli *

Institute of Inorganic Chemistry, Graz University of Technology, Stremayrgasse 9, 8010 Graz, Austria; b.schmidbauer@tugraz.at (B.S.); frank.uhlig@tugraz.at (F.U.)
* Correspondence: angela.chemelli@tugraz.at

Abstract: Nanostructured non-lamellar lipid particles are widely studied in various fields of application, although their self-assembled structure is sensitive to internal and external conditions, which may limit their applicability. The aim of this study was to overcome these limitations and create particles with non-lamellar nanostructures which are stable over time, upon drying and heating. This was achieved by the combination of two approaches: self-assembly of lipids and polymerization of alkoxysilanes. Precursors containing one or two unsaturated acyl chains were functionalized with trialkoxysilane headgroups. Contrarily to previous studies, the use of unsaturated acyl chains led to the formation of hybrid particles with non-lamellar internal nanostructures. These particles showed a sponge or a hexagonal arrangement and were named spongosomes and hexosomes. Due to the covalent linking of the precursors, durable structures were obtained. The particles were stable for at least several months and maintained their nanostructures even when they were dried or exposed to high temperatures. The inorganic functionalization of lipids enabled the fixation of the self-assembled nanostructures.

Keywords: self-assembly; spongosome; hexosome; non-lamellar; hybrid particle

Citation: Schmidbauer, B.; Uhlig, F.; Chemelli, A. Lipid–Inorganic Hybrid Particles with Non-Lamellar Structures. *Nanomanufacturing* **2022**, 2, 98–111. https://doi.org/10.3390/nanomanufacturing2030008

Academic Editor: Andres Castellanos-Gomez

Received: 28 June 2022
Accepted: 27 July 2022
Published: 2 August 2022

1. Introduction

Nanostructured non-lamellar lipid assemblies are widely studied in various fields of application such as vehicles for drug delivery [1–7], anti-microbial agents [8], biosensing [9] and nano-reactors [10]. Lipid-based materials and particles with bicontinuous cubic, hexagonal, micellar cubic, micellar structure and sponge phase can be formed by monoacylglycerols [11–20]. These self-assembled structures are stable in an excess of water, which enables the preparation of internally structured, non-lamellar particles in a continuous aqueous phase [21]. The resulting nanostructure depends on various parameters, particularly, lipid composition [22,23], additives [24–27], the composition of the aqueous phase [28] and temperature [29]. The adaptability of the structure facilitates its tailoring to the desired application. Depending on their internal structure, these materials, show distinct diverse properties. The nano-scaled structure affects their rheological behavior [29,30], water content [24] and, most importantly, release properties [6,31]. The sensitivity of the internal structure to external stimuli on one hand makes these materials interesting candidates in drug delivery applications [32–34], while, on the other hand, the sensitivity of the self-assembled phase may be disadvantageous and limits their applicability. Although the structure can be tailored, alterations of the above-mentioned influencing factors in their field of action will subsequently result in structural changes. Glycerol monooleate, for example, shows fast lipid mixing with model membranes [35]. This exchange of lipid molecules results in massive hemolysis of red blood cells [35].

Alkoxysilanes have been widely used for the preparation of nanostructured inorganic–organic hybrid materials [36]. The circumstance that alkoxysilanes undergo hydrolysis and polycondensation reactions, forming covalent bonds between monomers, facilitates the preservation of self-assembled structures. Siloxane-based materials with well-defined nanostructures have been studied for various applications such as membranes, drug

delivery, templates for nanoparticle synthesis and surfaces for catalysts [37–41]. It was established that they can encapsulate drugs [41] and have good biocompatibility [42,43]. The molecular design of these materials, involving changes in their characteristics such as composition, surface area, morphology and structure, is essential to meet the needs of the desired applications. The controlled growth of structured material can be directed either by surfactants [43–48] or by the self-assembly of amphiphilic precursors [47]. Higher uniformity and less defects can be achieved by a self-directed assembly process. Single molecular components of amphiphilic precursors containing e.g., alkoxysilyl functional groups self-assemble in aqueous solution. By subsequent hydrolysis and polycondensation, nanostructured materials are formed [36] in which the monomers are covalently connected by siloxane bonds. Materials with varying structures with hexagonal, monoclinic or cubic symmetry have been synthesized by this route, in which the organic residues are surrounded by siloxane [48–51]. Additionally, the formation of lamellar phases and vesicles from different precursors has been studied [52,53].

In the present study, the formation of nanostructured, non-lamellar lipid particles, comparable to those formed by unsaturated monoacylglycerols, and the preservation of the structure through alkoxysilane-functionalized precursors were combined, aiming at the formation of durable non-lamellar structures which will be preserved in the dry state and upon heating. Precursors containing hydrophobic unsaturated acyl tails, originating from unsaturated, long-chain fatty acid, were functionalized with trialkoxysilane headgroups. They were formed by connecting oleoyl residues to aminoalkylalkoxysilanes. The amide group formed from the primary amine and the resulting hydrogen bonds between the molecules will provide additional stability and support the self-assembly process. Although comparable precursors have already been studied, former research was limited to molecules with saturated hydrocarbon residues and resulting lamellar phases [54–59].

In contrast, the utilization of unsaturated lipid residues in this study gave rise to the formation hybrid particles with two non-lamellar nanostructures, namely, sponge and hexagonal H_2 phases. These so-called spongosomes and hexosomes showed a durable nanostructure which was maintained upon drying and exposure to high temperatures. The introduction of a double bond in *cis* conformation changed the geometry of the hydrophobic part of the precursors [60] and resulted in the formation of these non-lamellar phases. Further increase of the hydrophobic part was achieved by the attachment of a second unsaturated acyl chain. These lipid–inorganic hybrid materials were dispersed in water, forming nanostructured particles, comparable to nanostructured lipid particles.

2. Materials and Methods

2.1. Materials

Oleic acid (purity > 99%, TCI Chemicals, TCI Deutschland GmbH, Eschborn Germany), Oxalylchloride (98%, Acros organics, Fisher Scientific GmbH, Schwerte, Germany), and N,N-dimethylformamide (DMF, >99%, Drogerie Plomer, Graz, Austria) were used without further purification. The compounds (3-aminopropyl)trimethoxysilane (APTMS, >99%, Alfa Aesar, Fisher Scientific GmbH, Schwerte, Germany) and N-[3-(trimethoxysilyl)propyl]ethylenediamine (>99%, Evonik, Vienna, Austria) were distilled prior to use. Triethylamine (TEA, 99.5%, Roth Chemicals, Carl Roth GmbH + Co. KG, Karlsruhe, Germany) was distilled over KOH beforehand. The organic solvents pentane (Carl Roth GmbH + Co. KG, Karlsruhe, Germany) and dichloromethane (DCM, >99%, VWR Chemicals, VWR International, Vienna, Austria) were dried in advance. Hydrochloric acid (37%, VWR Chemicals, VWR International, Vienna, Austria) and sodium hydroxide (98.8%, VWR Chemicals, VWR International, Vienna, Austria) were used for adjusting the pH. Deionized water was used in all experiments. The ion-exchange resin Amberlyst® A-21 (Acros Chemicals, Fisher Scientific GmbH, Schwerte, Germany) was flushed with pentane and dried at 75 °C before it was used.

2.2. Synthesis of the Precursors

Oleoyl chloride was synthesized beforehand under inert conditions as described in the literature [61]. Oleic acid (11 mmol, 1.0 eq) was dissolved in 15 mL of dichloromethane (DCM) containing one drop of dimethylformamide (DMF). Subsequently, oxalyl chloride (13 mmol, 1.2 eq), dissolved in 6.4 mL of DCM, was added dropwise. The reaction mixture was stirred for two hours. Afterwards, the solvent was removed by evaporation, and the crude product was purified by vacuum distillation (yield 84%).

A general scheme of the synthesis of precursors A and B is shown in Figure 1. Precursor A was synthesized by adapting a well-known procedure [54–58] under inert conditions (Figure 1, precursor A). Oleoyl chloride (12 mmol) and 2 mL of triethylamine (TEA, 14 mmol) were dissolved in 30 mL of pentane and cooled by the help of an ice bath to 0 °C throughout the whole reaction. The compound (3-aminopropyl)trimethoxysilane (APTMS, 5 mL, 24 mmol) was dissolved in 20 mL of pentane and added to the cold oleoyl chloride solution dropwise. Afterwards, the ice bath was removed, and the solution was stirred overnight. Triethylammoniumchloride was removed by filtration, and the solvent was removed by evaporation. The remaining APTMS was removed by evaporation under reduced pressure (yield 90%).

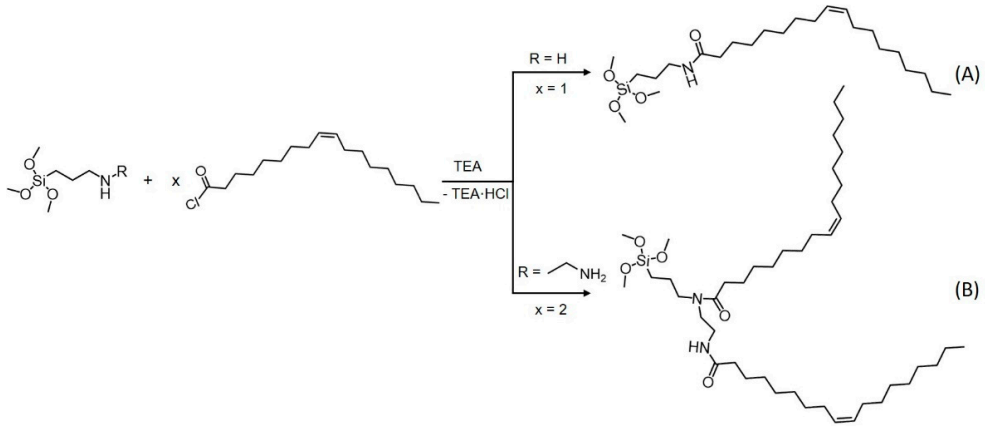

Figure 1. General scheme of the synthesis of precursors A and B from oleoyl chloride. Triethylamine was used to functionalize the acyl chloride with trialkoxysilanes.

To further expand the hydrophobic part of the precursors, a second oleoyl chain was connected (precursor B). In the amide group, the electrons of nitrogen were withdrawn by the carboxyl group. Thus, the attachment of a second acyl group to the amide in product A (Figure 1) was hindered. Therefore, a second acyl group was attached by connecting two equivalents of oleoyl chloride to *N*-[3-(trimethoxysilyl)propyl]ethylenediamine (Figure 1, precursor B) according to a procedure adapted to the synthesis described in the literature [59]. The reaction was performed under inert conditions. *N*-(2-Aminoethyl)-3-aminopropyltrimethoxysilane (2.8 mmol) was dissolved in 20 mL of pentane. The solution was cooled to 0 °C in an ice bath. Triethylamine (1.1. mmol) and the ion-exchange resin Amberlyst® A-21 (1.13 g, 5.6 mmol) were added to the solution. Oleoyl chloride (6.6 mmol), dissolved in 15 mL of pentane, was added dropwise to the solution. Afterwards, the solution was removed from the ice bath and stirred overnight. Triethylammoniumchloride and the ion-exchange resin were removed by filtration, and the solvent was removed by evaporation (yield 87%). The successful synthesis of both precursors was verified by NMR (^{1}H (Figures S1, S3, S6 and S7), ^{13}C (Figures S2, S4 and S8), ^{29}Si (Figures S5 and S9)) and FT-IR measurements (Figures S10–S12)).

2.3. Preparation of Nanostructured Particles

Nanostructured particles were prepared by mixing the precursors with aqueous solutions. Hydrolysis and polycondensation of the alkoxysilanes were catalyzed by either acidic or basic conditions. The pH was adjusted to 1.3 by hydrochloric acid or to 11.6 by

sodium hydroxide. The particles were prepared by vigorously stirring 5 mL of aqueous solution with a magnetic stirrer and slowly adding 0.5 g of the precursor. The dispersions were stirred for a day, and the samples were allowed to equilibrate for one week at ambient conditions before they were subjected to measurement. The measurements were repeated after storing the samples at ambient conditions for 10–12 months.

2.4. Characterization of Nanostructured Particles

Nanostructured particles were characterized by small- and wide-angle X-ray scattering (SAXS, WAXS), dynamic light scattering (DLS), zeta-potential measurements and atomic force microscopy (AFM).

The SAXS equipment consisted of a SAXSess camera (Anton-Paar GmbH, Graz, Austria). The X-ray source was a sealed-tube X-ray generator (DebyeFlex3000) operating at 40 kV and 50 mA. The divergent polychromatic X-ray beam was focused into a line-shaped beam of Cu Kα radiation (λ = 0.154 nm) with a Goebel mirror. A 1D-Diode detector (Mythen 1K, Dectris, Switzerland) was used to record the scattering patterns. It has 1280 pixels, each having a size of 50 µm. The samples were introduced into a capillary. Measurements lasting 10 seconds were recorded 180 times. SAXS/WAXS measurements of the aged and dried samples were measured by a SAXSpoint 2.0 (Anton-Paar, Graz, Austria) containing a Primux 100 microfocus X-ray source operating at λ = 0.154 nm (Cu Kα). Two-dimensional scattering patterns were recorded by a 2D EIGER R series Hybrid Photon Counting (HPC) detector (Dectris Ltd., Baden-Daettwil, Switzerland). The samples were introduced into a capillary (1 mm diameter) or a paste cell and measured 10 times for 300 s. For the temperature scans, the samples were allowed to equilibrate for 40 min before they were measured 10 times for 120 s. The scattering patterns were averaged, edited by correcting the cosmic X-ray impacts and integrated to obtain one-dimensional scattering patterns.

DLS and zeta-potential measurements of the nanostructured particles were performed using a Litesizer 500 (Anton Paar GmbH, Graz, Austria). The samples were diluted by a factor of app. of 100 or 10 with water for size and zeta-potential measurements, respectively. The samples were allowed to equilibrate at 25 °C for at least five minutes before the measurements were performed. Dynamic light scattering was measured at an angle of 90° or 175°. The Kalliope^{TM} software (Anton Paar GmbH, Graz, Austria) was used for measurement and data evaluation. The advanced cumulant model was applied for the calculation of the mean hydrodynamic radius and the polydispersity index (PDI).

The atomic force microscope Tosca 400 (Anton Paar GmbH, Graz, Austria) was used to capture the morphology of the dried samples. Tapping-mode imaging was performed using highly doped monolithic silicon cantilevers with an approximate force constant of 42 N/m and a resonance frequency of app. of 285 kHz. The samples were dripped on mica discs and dried at ambient conditions over night. The images (topography, amplitude and phase) were recorded with a resolution of 400 × 400 and a scanning speed of 0.3–1 line/s.

3. Results

3.1. Formation of Structures and Their Evolution over Time

The effect of the introduction of the *cis* double bond on the structures was determined by SAXS measurements. Both precursors could be dispersed in aqueous solutions. The SAXS patterns showed that the particles formed contained different internal nanostructures depending on the precursor. The SAXS pattern of the sample containing precursor A showed a broad correlation peak, related to the correlation length of 4.0 nm (Figure 2). To identify the structure formed, further investigations were necessary. Performing the experiment with precursor A in acidic conditions led to a mixed-phase system. Two structures were found in the SAXS measurements (Figure 2). The first structure showed equidistant peaks corresponding to a lamellar structure having an interlamellar spacing of 5.8 nm, which was already found in comparable systems with saturated acyl residues [54]. Additionally, the broad correlation peak that was also found under basic reaction conditions, referring to the correlation length of 4.0 nm, could be observed. The SAXS patterns

of sponge phases possess such broad correlation peaks, originating from bilayer correlations [16], whose size corresponds to the sum of the bilayer thickness and the water channel [62]. Assuming comparable bilayer thicknesses and concentrations of lipids in the two-phase system mentioned above, a ratio of q (correlation peak)/q (lamellar phase) of 1.5 was predicted theoretically [63] and observed experimentally [64] for sponge phases. In the current example a value of 1.45 was observed for these particles, indicating the existence of a sponge phase.

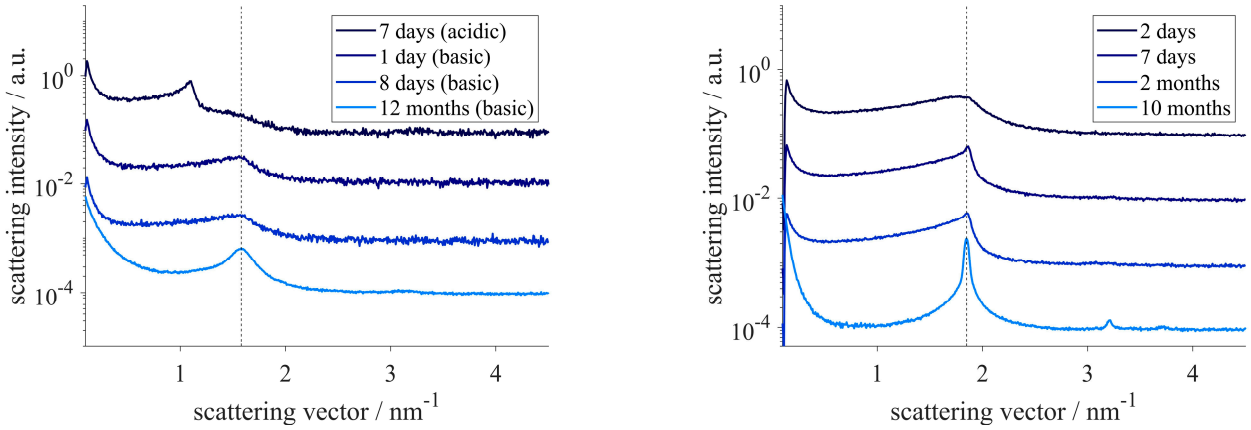

(**a**) (**b**)

Figure 2. SAXS-pattern of nanostructured particles of precursor A (**a**) and precursor B (**b**) at different times after preparation under acidic or basic conditions. The dotted lines indicate the correlation peak of the sponge phase at q = 1.58 nm^{-1} (**a**) or the location of the first peak of the hexagonal phase at q = 1.85 nm^{-1} (**b**).

The structure formed by precursor A was fully developed after one day and was stable for at least 12 months (Figure 2). The hydrodynamic radius of 47 nm (PDI 22%) of these particles, also referred to as spongosomes, was maintained for at least 12 months.

The development of the structure assembled by precursor B was slower compared to that of the sponge phase. After two days, a broad correlation peak, referring to a correlation length of 3.5 nm, was observed. Within a week, peaks associated with a hexagonal symmetry evolved. A lattice constant of 3.9 nm was determined for this structure from the SAXS measurements. Even after 10 months, the structure was maintained, and no change in the lattice constant was detected. Beside the formation of few larger aggregates, these so-called hexosomes showed a hydrodynamic radius of 240 nm (PDI 33%) even 10 months after their preparation. The spongosomes and the hexosomes exhibited a high surface charge, having a zeta-potential of -51 ± 3 mV and -89 ± 2 mV, respectively, which prevented the aggregation of the particles.

3.2. Drying and Rehydration

Additionally, to the spongosomes' and hexosomes' stability over time, the resistance to drying of their structures was also assessed. Therefore, the spongosomes and hexosomes were dried under ambient conditions, and their nanostructure was determined. Although a slight shrinking of both structures could be observed in the SAXS measurements, their structure was maintained. The correlation length of the sponge phase shrank to 3.9 nm. A minimal decrease of less than 0.1 nm in the lattice constant could also be found for the hexosomes. The reversibility of the shrinkage was examined by rehydrating the samples. The initial structural sizes were recovered within minutes (Figure 3).

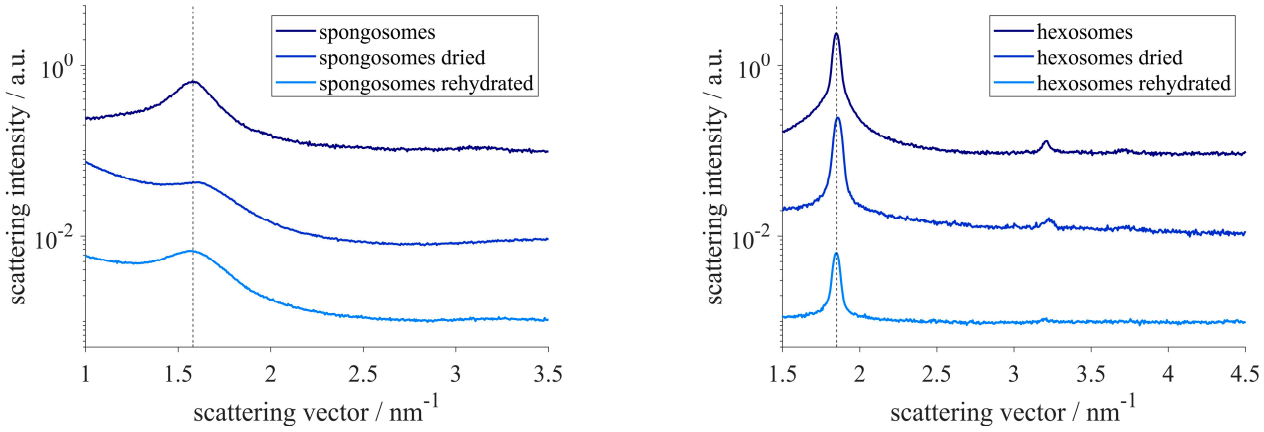

(**a**) (**b**)

Figure 3. SAXS-pattern of spongosomes (**a**) and hexosomes (**b**) after drying and rehydration at ambient conditions. The dotted lines indicate the correlation peak of the sponge phase (**a**) and the hexagonal phase (**b**) of the pristine particles at q = 1.58 nm^{-1} and q = 1.85 nm^{-1}, respectively.

Additionally, WAXS measurements of the dry samples were performed. In both samples, a broad correlation peak at a scattering vector of approximately 14 nm^{-1} could be observed (Figure 4). The corresponding correlation length of the spongosomes was slightly smaller (0.44 nm) compared to the one found in the hexosome sample (0.45 nm). The measured values are in accordance with the distance between the silicon atoms in the siloxane backbone [54]. Interestingly, a sharp peak at q = 22.4 nm^{-1}, corresponding to a correlation length of 0.28 nm, was only detected in the sample having the hexagonal structure. Because this was the only sharp peak measured, it was not possible to evaluate its origin.

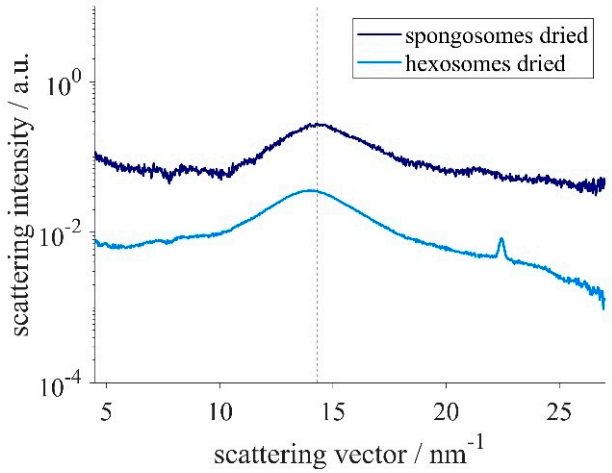

Figure 4. WAXS pattern of dried spongosomes and hexosomes. The dotted line indicates the correlation peak of the sponge phase at q = 14.29 nm^{-1}.

Since the structure was preserved in the dry state, AFM pictures of the dried spongosomes and hexosomes were recorded (Figure 5). The spherical shape of the spongosomes was shown to be stable upon drying. The continuous structure of the spongosomes resulted in particles that did not collapse. The AFM pictures showed particles sizes of around 100 nm, in accordance with the size of the particles in suspension measured by DLS. More inhomogeneous particle sizes were observed for the hexosomes, with a maximum size of up to 1 µm.

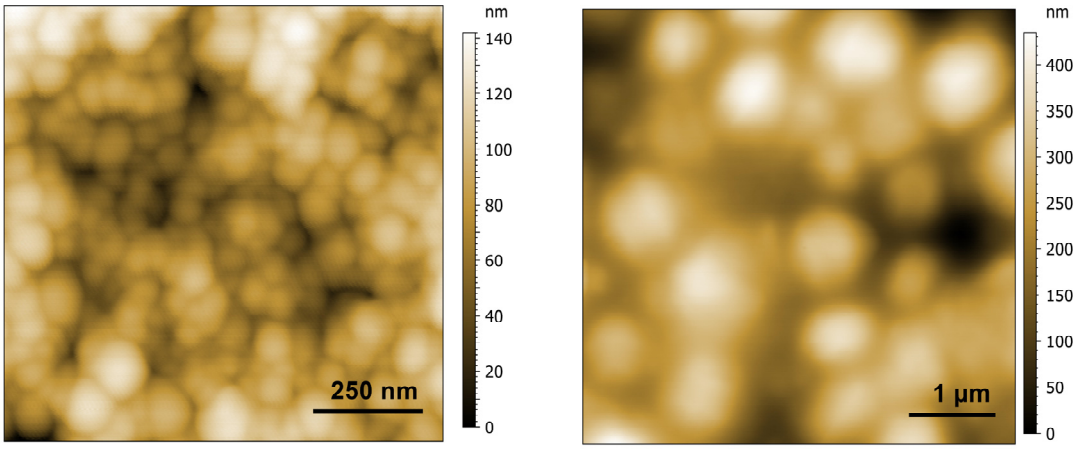

(**a**) (**b**)

Figure 5. AFM topography pictures of spongosomes (**a**) and hexosomes (**b**) after drying.

For a better visibility of the shape of the particles, AFM pictures of the measured amplitude are shown in Figure 6. The particles had more irregular, edged shapes, as seen in the amplitude image. Curved striations were visible, comparable to those observed for hexosomes formed of phytantriol, as reported previously [65].

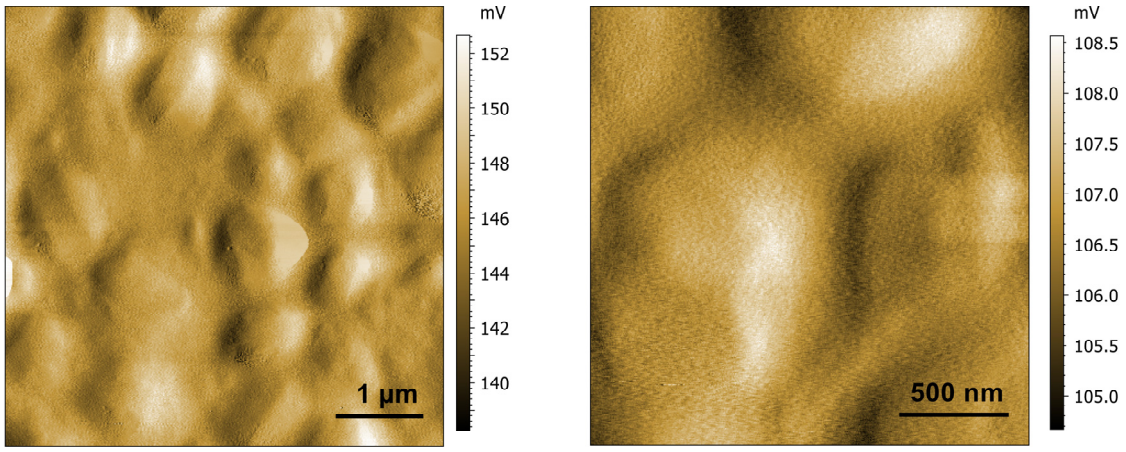

(**a**) (**b**)

Figure 6. AFM amplitude pictures of hexosomes after drying at different resolutions (**a**,**b**).

3.3. Stability upon Temperature Increase

To assess the applicability of the samples over a broad temperature range, the particles were exposed to high temperatures (Figure 7). The structure parameters, i.e., the lattice constant in the case of hexosomes and the correlation length for spongosomes, decreased when the samples were heated above 100 °C. This was associated with a shrinkage of the hexagonal structure when the temperature increased above 100 °C. As the temperature raised, the shrinking slowed down. The spongosomes showed only slight structural shrinking up to 150 °C, as can be observed by a hardly changing correlation length. As the temperature increased from 150 °C to 180 °C, the correlation length dropped by approximately 10%.

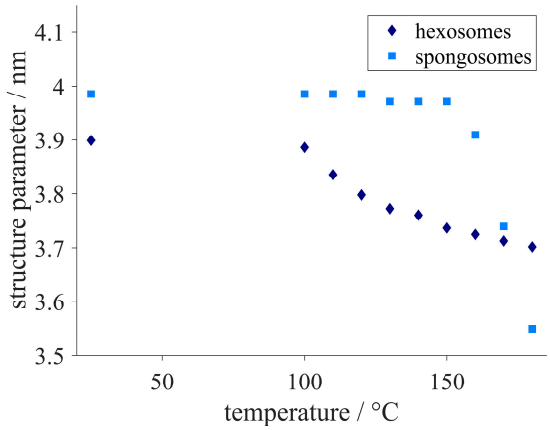

Figure 7. Changes in structure parameters, i.e., the lattice constant in the case of hexosomes (diamonds) and the correlation length for spongosomes (squares), when heating the samples up to 180 °C.

The structural changes that occurred when heating the samples to 180 °C were not reversible upon rehydration, as it was found for the samples which were dried under gentle conditions (Figure 8). The SAXS pattern showed that the correlation length and lattice constant of the spongosomes and hexosomes, respectively, were not recovered when the samples were equilibrated in water. Particles heated to 180 °C not only lost the physically adsorbed water, but also could undergo chemical changes [66], consisting in the remaining silanol groups undergoing condensation reactions to form siloxane.

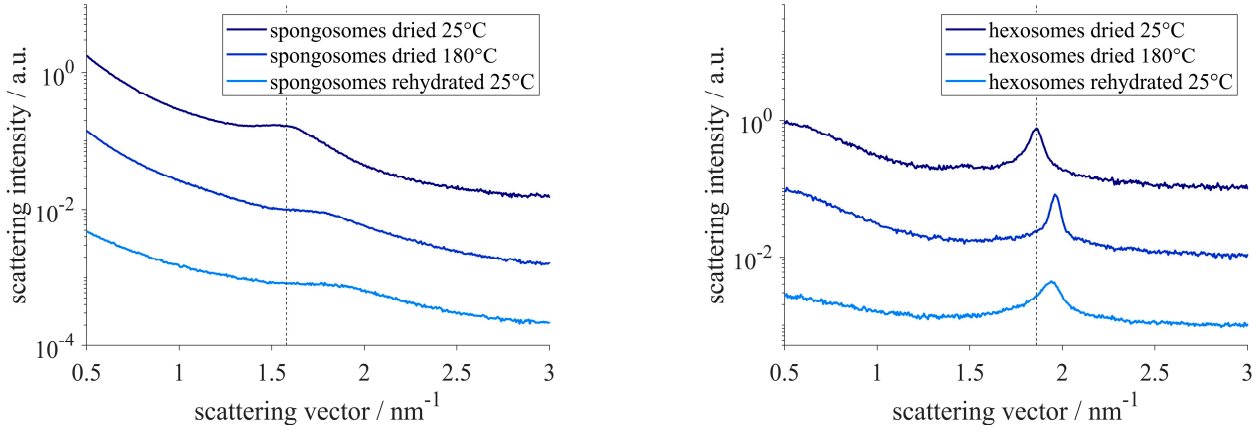

Figure 8. SAXS-pattern of spongosomes (**a**) and hexosomes (**b**) after drying, heating to 180 °C and rehydration. The dotted lines indicate the correlation peak of the sponge phase (**a**) and the hexagonal phase (**b**) at q = 1.58 nm^{-1} and q = 1.86 nm^{-1}, respectively, of the dried particles at 25 °C.

4. Discussion

Acyl residues functionalized with trialkoxysilanes acted as precursors for the formation of non-lamellar nanostructured particles. As the precursors became in contact with water, hydrolysis and polycondensation occurred (Figure 9). To ensure a fast water saturation of the self-assembled phase and the exchange of reaction products, i.e., the alcohol produced during the hydrolysis reaction, the precursors were dispersed in aqueous solution to form these nanostructured particles. In neutral aqueous solution, the kinetics of those chemical reactions were slow. To increase the reaction rate, these steps can be catalyzed by acidic or basic conditions [67].

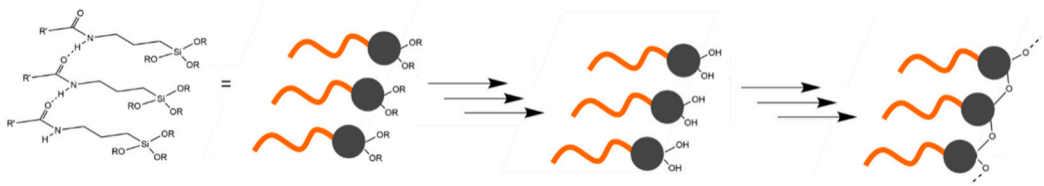

Figure 9. Schematic drawing of hydrolysis and polycondensation.

In acidic conditions, hydrolysis is slow compared to polycondensation, thus being the rate-determining step. The opposite observation was made in basic conditions. In this case. the reaction rate is determined by the polycondensation step [67]. As the precursors hydrolyze, silanol groups form. The higher hydrophilicity of the silanol groups supports the self-assembly process of the precursor molecules. Therefore, basic reaction conditions were chosen to catalyze these reactions. Comparable precursors with saturated acyl residues are known to form lamellar structures [54–59]. The oleoyl chain contains a double bond in *cis* conformation, which led to changes in the packing of the precursor molecules. A concept to predict the optimal packing geometry from a few molecular parameters, the so-called critical packing parameter (CPP), relates the volume of the hydrophobic tail to the product of the hydrophobic chain length and the area of the hydrophilic head group [68]. The introduction of a double bond in *cis* conformation changed the geometry of the hydrophobic part of the precursors and resulted in an alteration of the structure [60]. Increasing the negative interfacial curvature from the lamellar phase, a transformation to inverse lipid mesophases with other continuous structures was induced [69]. The space requirement of the alkyl chain was altered because of the bend in the chain caused by the *cis* double bond. The resulting increase in negative interfacial curvature caused that molecules of precursor A to arrange in a sponge phase, resulting in particles with an internal sponge structure that were called spongosomes. While cubic structures possess ordered continuous networks of water channels, the sponge phase is characterized by an irregular three-dimensional membrane structure [16,23]. A schematic representation of the possible molecular arrangements is shown in Figure 10.

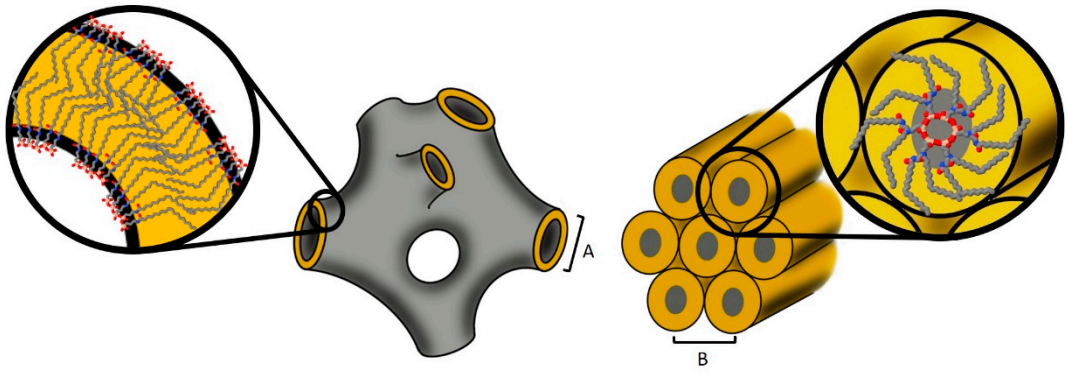

Figure 10. Schematic drawing of possible molecular arrangements in the sponge phase (left drawing, A: correlation length) and the hexagonal structure (right drawing, B: lattice constant).

The structure of the spongosomes was fully developed after one day. During that time, the precursors underwent hydrolysis, forming silanol functional groups. The increased hydrophilicity of the silanols with respect to that of the alkolysilanes caused the self-assembly of the precursor molecules into the aforementioned sponge phase. The structure that formed within the first day of preparation was confirmed even 12 months later.

The hydrophobic part of the precursors was further increased by the introduction of a second oleoyl residue (precursor B). While such precursors containing saturated residues form a hierarchical architecture composed of two lamellar bilayer structures [59], the used precursor formed a hexagonal structure. Compared to the sponge phase, the formation of the hexagonal structure was slower. The hexagonal arrangement was developed within one

week. Lipid assemblies with hexagonal structure show hexagonally arranged elongated micelles, which suggested that the current hexosomes were also composed of rod-like subunits, with the reactive headgroups pointing towards the core [70,71] (see Figure 10). Additionally, the precursors had higher hydrophobicity because of the two acyl chains. The reduced accessibility of the head groups in this case could be responsible for the slower formation of the structure. The polycondensation of precursor B resulted in rod-like core–shell structures with silica cores and organic shells. Organosilanes were reported to form similar core–shell nano-fibers arranged in hexagonal structures [70]. In that case, the hexagonal structure was achieved by the incorporation of additives. In contrast, the hexagonal structure in the present study was directed solely by the precursor molecules [71] and was stable in aqueous environment. Both precursors A and B possess three methoxy groups per molecule which can undergo chemical reactions and form Si-O-Si connecting covalent bonds. The three functionalities are, in principle, able to form a three-dimensional network. This covalent linking between the molecules facilitates the preservation of the structures and of the particles. The spongosomes and hexosomes maintained their particle size and structure in dispersion for at least 10 months. They even maintained their nanostructure when they were dried. The minor shrinking and recovery of the structure upon drying and rehydration indicated that the network was not completely rigid and exhibited a slight flexibility. In contrast, the structure could not be rehydrated when the particles were dried and heated up to 180 °C. In this case, the nanostructure of the spongosomes as well as of the hexosomes shrank. The shrinking of the hexagonal structure occurred at temperatures higher than 100 °C. The correlation length of the spongosomes was hardly affected by temperatures up to 150 °C. Heating the sample above this temperature caused a shrinking of the structure, which was more pronounced compared to that occurring in the hexosomes. After the heat treatment, both nanostructures did not recover upon rehydration. Higher temperatures induced the condensation of the remaining Si-OH groups [66]. This enhanced crosslinking of the precursors hindered the incorporation of water and the subsequent swelling of the structures. The particles in this study showed hexagonal and sponge structures comparable to those formed by the self-assembly of lipids (see Table 1). In comparison to these latter structures, the nanostructures prepared in this study exhibited improved stability and could be prepared at various water contents and in a broad range of temperatures.

Table 1. Comparison of inverse hexagonal and sponge structures of particles created in this study to those derived from the self-assembly of lipids, with respect to their feasible water content and temperature range.

Nanostructure	Covalent Connection between Monomers	Water Content	Temperature Range	References
inverse hexagonal	no	16–26%	82 °C–100 °C	[72]
inverse hexagonal	yes	0%–saturated [1]	<25 °C–>180 °C	this study (precursor A)
sponge phase	no	60%–saturated [1]	not determined	[17]
sponge phase	yes	0%–saturated [1]	<25 °C–>180 °C	this study (precursor B)

[1] Hexosomes and spongosomes were prepared in excess aqueous phase.

In contrast to previous studies in which comparable precursors with saturated acyl residues were used, in this work, non-lamellar nanostructures were formed by incorporating oleoyl-groups (Table 2).

Table 2. Comparison of the nanostructures formed depending on the type and number of acyl residues in the precursor molecules.

Nanostructure	Structure Parameter [2]	Acyl Residue	Number of Acyl Residues Per Precursor Molecule	References
lamellar	5.42 nm	palmitoyl	1	[54]
sponge	4.0 nm	oleoyl	1	this study (precursor A)
lamellar	4.72 nm and 3.15 nm	myristoyl	2	[59]
inverse hexagonal	3.9 nm	oleoyl	2	this study (precursor B)

[2] Bilayer spacing, lattice constant or correlation length for lamellar, inverse hexagonal or sponge structures, respectively.

Spongosomes and hexosomes in this study showed stability over time, upon drying and heating. In the spongosome and hexosome dispersions, only minor aggregation occurred within month. This was ascribed to the high surface charge and resulting repulsive interaction between the particles. Additionally, their internal structure was also maintained in this time period. The trialkoxysilyl functionality of the precursor molecules underwent hydrolysis and polycondensation. The formed covalent bonds between the monomers indicated remarkable stability of the nanostructures. Upon drying and heating, both nanostructures shrank, but no transformation or loss of the phases occurred.

5. Conclusions

Lipid–inorganic hybrid particles can be prepared using a simple method by dispersing precursors in basic aqueous solutions. The composition and consequently the geometry of the precursor molecules influenced the internal nanostructure of the formed particles. While previous studies were limited to the use of saturated acyl residues forming lamellar phases, the current study shows the formation of non-lamellar structures. A sponge phase formed when the precursor contained one oleoyl side chain, and a hexagonal structure was synthesized when the precursor contained two of these groups. Spongosomes and hexosomes, which derived solely from the self-assembly of lipids, are sensitive to various parameters such as water content and temperature. Contrarily, the precursors produced in this study formed particles in which the monomers were covalently linked. This resulted in durable structures that were maintained in dry state and at high temperatures. These particles can therefore be used with varying water content and in a broad temperature range, without transformation or loss of the nanostructure.

Supplementary Materials: The following supplementary information can be downloaded at: https://www.mdpi.com/article/10.3390/nanomanufacturing2030008/s1. Figure S1: ^{1}H-NMR Spectra of the distilled oleoyl chloride in $CDCl_3$, Figure S2: ^{13}C-NMR Spectra of the distilled oleoyl chloride in $CDCl_3$, Figure S3: ^{1}H-NMR Spectra of N-[3-(trimethoxysilyl)propyl]oleamide in $CDCl_3$, Figure S4: ^{13}C-NMR Spectra of N-[3-(trimethoxysilyl)propyl]oleamide in $CDCl_3$, Figure S5: ^{29}Si-DEPT-NMR Spectra of N-[3-(trimethoxysilyl)propyl]oleamide in $CDCl_3$, Figure S6: ^{1}H-NMR Spectra of the N-[2-(oleoylamino)ethyl]-N-[3-(trimethoxysilyl)propyl]oleamide in $CDCl_3$, Figure S7: ^{1}H-NMR Spectra (from 5.5 to 3.0 ppm) of the N-[2-(oleoylamino)ethyl]-N-[3-(trimethoxysilyl)propyl]oleamide in $CDCl_3$, Figure S8: ^{13}C-NMR Spectra of N-[2-(oleoylamino)ethyl]-N-[3-(trimethoxysilyl)propyl]oleamide in $CDCl_3$, Figure S9: ^{29}Si-DEPT-NMR Spectra of N-[2-(oleoylamino)ethyl]-N-[3-(trimethoxysilyl)propyl]oleamide in $CDCl_3$, Figure S10: FT-IR-Spectra of polymer derivates from N-[2-(oleoylamino)ethyl]-N-[3-(trimethoxysilyl)propyl]oleamide, Figure S11: FT-IR-Spectra of polymer derivates from N-[3-(trimethoxysilyl)propyl]oleamide, Figure S12: FT-IR-Spectra comparison of polymer derivates from N-[2-(oleoylamino)ethyl]-N-[3-(trimethoxysilyl)propyl]oleamide (blue) and N-[3-(trimethoxysilyl)propyl]oleamide (orange).

Author Contributions: Conceptualization, A.C. and F.U.; methodology, A.C. and F.U.; investigation, A.C. and B.S.; resources, F.U.; data curation, A.C. and B.S.; writing—original draft preparation, A.C.; writing—review and editing, B.S. and F.U.; supervision, A.C. and F.U.; project administration, A.C. and F.U. All authors have read and agreed to the published version of the manuscript.

Funding: The authors also acknowledge initial support by funding from the TU Graz Field of Expertise 'Advanced Material Science'.

Data Availability Statement: Measurement data available upon request to the corresponding author.

Acknowledgments: The authors would like to acknowledge the use of the Somapp-Lab, a core facility supported by the Austrian Federal Ministry of Education, Science and Research, the Graz University of Technology, the University of Graz and Anton Paar GmbH.

Conflicts of Interest: The authors declare no conflict of interest.

References

1. Amar-Yuli, I.; Azulay, D.; Mishraki, T.; Aserin, A.; Garti, N. The role of glycerol and phosphatidylcholine in solubilizing and enhancing insulin stability in reverse hexagonal mesophases. *J. Colloid Interface Sci.* **2011**, *364*, 379–387. [CrossRef] [PubMed]
2. Bender, J.; Simonsson, C.; Smedh, M.; Engström, S.; Ericson, M.B. Lipid cubic phases in topical drug delivery: Visualization of skin distribution using two-photon microscopy. *J. Control. Release* **2008**, *129*, 163–169. [CrossRef] [PubMed]
3. Boyd, B.J.; Khoo, S.M.; Whittaker, D.V.; Davey, G.; Porter, C.J.H. A lipid-based liquid crystalline matrix that provides sustained release and enhanced oral bioavailability for a model poorly water soluble drug in rats. *Int. J. Pharm.* **2007**, *340*, 52–60. [CrossRef] [PubMed]
4. Libster, D.; Ishai, P.B.; Aserin, A.; Shoham, G.; Garti, N. Molecular interactions in reverse hexagonal mesophase in the presence of Cyclosporin A. *Int. J. Pharm.* **2009**, *367*, 115–126. [CrossRef]
5. Lopes, L.B.; Speretta, F.F.F.; Bentley, M.V.L.B. Enhancement of skin penetration of vitamin K using monoolein-based liquid crystalline systems. *Eur. J. Pharm. Sci.* **2007**, *32*, 209–215. [CrossRef]
6. Chemelli, A.; Maurer, M.; Geier, R.; Glatter, O. Optimized loading and sustained release of hydrophilic proteins from internally nanostructured particles. *Langmuir* **2012**, *28*, 16788–16797. [CrossRef]
7. Milak, S.; Chemelli, A.; Glatter, O.; Zimmer, A. Vancomycin ocular delivery systems based on glycerol monooleate reversed hexagonal and reversed cubic liquid crystalline phases. *Eur. J. Pharm. Biopharm.* **2019**, *139*, 279–290. [CrossRef]
8. Zabara, M.; Senturk, B.; Gontsarik, M.; Ren, Q.; Rottmar, M.; Maniura-Weber, K.; Mezzenga, R.; Bolisetty, S.; Salentinig, S. Multifunctional Nano-Biointerfaces: Cytocompatible Antimicrobial Nanocarriers from Stabilizer-Free Cubosomes. *Adv. Funct. Mater.* **2019**, *29*, 1904007. [CrossRef]
9. Fraser, S.J.; Dawson, R.M.; Waddington, L.J.; Muir, B.W.; Mulet, X.; Hartley, P.G.; Separovic, F.; Polyzos, A. Development of cubosomes as a cell-free biosensing platform. *Aust. J. Chem.* **2011**, *64*, 46–53. [CrossRef]
10. Duss, M.; Salvati Manni, L.; Moser, L.; Handschin, S.; Mezzenga, R.; Jessen, H.J.; Landau, E.M. Lipidic Mesophases as Novel Nanoreactor Scaffolds for Organocatalysts: Heterogeneously Catalyzed Asymmetric Aldol Reactions in Confined Water. *ACS Appl. Mater. Interfaces* **2018**, *10*, 5114–5124. [CrossRef]
11. De Campo, L.; Yaghmur, A.; Sagalowicz, L.; Leser, M.E.; Watzke, H.; Glatter, O. Reversible phase transitions in emulsified nanostructured lipid systems. *Langmuir* **2004**, *20*, 5254–5261. [CrossRef]
12. Guillot, S.; Moitzi, C.; Salentinig, S.; Sagalowicz, L.; Leser, M.E.; Glatter, O. Direct and indirect thermal transitions from hexosomes to emulsified micro-emulsions in oil-loaded monoglyceride-based particles. *Colloids Surfaces A Physicochem. Eng. Asp.* **2006**, *291*, 78–84. [CrossRef]
13. Tilley, A.; Dong, Y.-D.; Amenitsch, H.; Rappolt, M.; Boyd, B.J. Transfer of lipid and phase reorganisation in self-assembled liquid crystal nanostructured particles based on phytantriol. *Phys. Chem. Chem. Phys.* **2011**, *13*, 3026–3032. [CrossRef]
14. Yaghmur, A.; De Campo, L.; Sagalowicz, L.; Leser, M.E.; Glatter, O. Emulsified microemulsions and oil-containing liquid crystalline phases. *Langmuir* **2005**, *21*, 569–577. [CrossRef] [PubMed]
15. Yaghmur, A.; De Campo, L.; Salentinig, S.; Sagalowicz, L.; Leser, M.E.; Glatter, O. Oil-loaded monolinolein-based particles with confined inverse discontinuous cubic structure (Fd3m). *Langmuir* **2006**, *22*, 517–521. [CrossRef]
16. Angelov, B.; Angelova, A.; Mutafchieva, R.; Lesieur, S.; Vainio, U.; Garamus, V.M.; Jensen, G.V.; Pedersen, J.S. SAXS investigation of a cubic to a sponge (L3) phase transition in self-assembled lipid nanocarriers. *Phys. Chem. Chem. Phys.* **2011**, *13*, 3073–3081. [CrossRef] [PubMed]
17. Valldeperas, M.; Wiśniewska, M.; Ram-On, M.; Kesselman, E.; Danino, D.; Nylander, T.; Barauskas, J. Sponge Phases and Nanoparticle Dispersions in Aqueous Mixtures of Mono- and Diglycerides. *Langmuir* **2016**, *32*, 8650–8659. [CrossRef]
18. Gilbert, J.; Ermilova, I.; Nagao, M.; Swenson, J.; Nylander, T. Effect of encapsulated protein on the dynamics of lipid sponge phase: A neutron spin echo and molecular dynamics simulation study. *Nanoscale* **2022**, *14*, 6990–7002. [CrossRef]
19. Zhai, J.; Sarkar, S.; Conn, C.E.; Drummond, C.J. Molecular engineering of super-swollen inverse bicontinuous cubic and sponge lipid phases for biomedical applications. *Mol. Syst. Des. Eng.* **2020**, *5*, 1354–1375. [CrossRef]
20. Valldeperas, M.; Talaikis, M.; Dhayal, S.K.; Velička, M.; Barauskas, J.; Niaura, G.; Nylander, T. Encapsulation of Aspartic Protease in Nonlamellar Lipid Liquid Crystalline Phases. *Biophys. J.* **2019**, *117*, 829–843. [CrossRef]
21. Gustafsson, J.; Ljusberg-Wahren, H.; Almgren, M.; Larsson, K. Submicron Particles of Reversed Lipid Phases in Water Stabilized by a Nonionic Amphiphilic Polymer. *Langmuir* **1997**, *13*, 6964–6971. [CrossRef]

22. Johnsson, M.; Lam, Y.; Barauskas, J.; Tiberg, F. Aqueous phase behavior and dispersed nanoparticles of diglycerol monooleate/glycerol dioleate mixtures. *Langmuir* **2005**, *21*, 5159–5165. [CrossRef]
23. Yaghmur, A.; De Campo, L.; Sagalowicz, L.; Leser, M.E.; Glatter, O. Control of the internal structure of MLO-based isasomes by the addition of diglycerol monooleate and soybean phosphatidylcholine. *Langmuir* **2006**, *22*, 9919–9927. [CrossRef] [PubMed]
24. Salonen, A.; Guillot, S.; Glatter, O. Determination of water content in internally self-assembled monoglyceride-based dispersions from the bulk phase. *Langmuir* **2007**, *23*, 9151–9154. [CrossRef]
25. Garti, N.; Spernath, A.; Aserin, A.; Lutz, R. Nano-sized self-assemblies of nonionic surfactants as solubilization reservoirs and microreactors for food systems. *Soft Matter* **2005**, *1*, 206–218. [CrossRef]
26. Chemelli, A.; Conde-Valentín, B.; Uhlig, F.; Glatter, O. Amino Acid Induced Modification of Self-Assembled Monoglyceride-Based Nanostructures. *Langmuir* **2015**, *31*, 10377–10381. [CrossRef]
27. Guillot, S.; Salentinig, S.; Chemelli, A.; Sagalowicz, L.; Leser, M.E.; Glatter, O. Influence of the stabilizer concentration on the internal liquid crystalline order and the size of oil-loaded monolinolein-based dispersions. *Langmuir* **2010**, *26*, 6222–6229. [CrossRef]
28. Salentinig, S.; Sagalowicz, L.; Glatter, O. Self-assembled structures and pK a value of oleic acid in systems of biological levance. *Langmuir* **2010**, *26*, 11670–11679. [CrossRef]
29. Mezzenga, R.; Meyer, C.; Servais, C.; Romoscanu, I.; Sagalowicz, L.; Hayward, R.C.; Romoscanu, A.I. Shear Rheology of Lyotropic Liquid Crystals: A Case Study Shear Rheology of Lyotropic Liquid Crystals: A Case Study. *Liq. Cryst.* **2005**, *21*, 3322–3333. [CrossRef]
30. Kulkarni, C.V.; Mezzenga, R.; Glatter, O. Water-in-oil nanostructured emulsions: Towards the structural hierarchy of liquid crystalline materials. *Soft Matter* **2010**, *6*, 5615–5624. [CrossRef]
31. Phan, S.; Fong, W.K.; Kirby, N.; Hanley, T.; Boyd, B.J. Evaluating the link between self-assembled mesophase structure and drug release. *Int. J. Pharm.* **2011**, *421*, 176–182. [CrossRef]
32. Negrini, R.; Mezzenga, R. pH-responsive lyotropic liquid crystals for controlled drug delivery. *Langmuir* **2011**, *27*, 5296–5303. [CrossRef] [PubMed]
33. Prajapati, R.; Gontsarik, M.; Yaghmur, A.; Salentinig, S. PH-Responsive Nano-Self-Assemblies of the Anticancer Drug 2-Hydroxyoleic Acid. *Langmuir* **2019**, *35*, 7954–7961. [CrossRef] [PubMed]
34. Fong, W.K.; Hanley, T.; Boyd, B.J. Stimuli responsive liquid crystals provide "on-demand" drug delivery in vitro and in vivo. *J. Control. Release* **2009**, *135*, 218–226. [CrossRef]
35. Barauskas, J.; Cervin, C.; Jankunec, M.; Špandyreva, M.; Ribokaite, K.; Tiberg, F.; Johnsson, M. Interactions of lipid-based liquid crystalline nanoparticles with model and cell membranes. *Int. J. Pharm.* **2010**, *391*, 284–291. [CrossRef]
36. Kuroda, K.; Shimojima, A.; Kawahara, K.; Wakabayashi, R.; Tamura, Y.; Asakura, Y.; Kitahara, M. Utilization of alkoxysilyl groups for the creation of structurally controlled siloxane-based nanomaterials. *Chem. Mater.* **2014**, *26*, 211–220. [CrossRef]
37. Yue, X.; Dai, Z. Recent advances in liposomal nanohybrid cerasomes as promising drug nanocarriers. *Adv. Colloid Interface Sci.* **2014**, *207*, 32–42. [CrossRef]
38. Kikuchi, J.; Yasuhar, K. Cerasomes: A New Family of Artificial Cell Membranes with Ceramic Surface. In *Advances in Biomimetics*; InTech: Rijeka, Croatia, 2011. [CrossRef]
39. Fan, H.T.; Liu, X.G.; Xing, X.J.; Li, B.; Wang, K.; Chen, S.T.; Wu, Z.; Qiu, D.F. Ordered mesoporous silica cubic particles decorated with silver nanoparticles: A highly active and recyclable heterogeneous catalyst for the reduction of 4-nitrophenol. *Dalton Trans.* **2019**, *48*, 2692–2700. [CrossRef]
40. Zeng, J.; Zhou, Y.; Li, L.; Jiang, S.P. Phosphotungstic acid functionalized silica nanocomposites with tunable bicontinuous mesoporous structure and superior proton conductivity and stability for fuel cells. *Phys. Chem. Chem. Phys.* **2011**, *13*, 10249–10257. [CrossRef]
41. Wang, Y.; Chen, Y.; Zhang, M.; Qu, H.; Zheng, J.; Pang, Q.; Yan, X. Safety evaluation of liposomal nanohybrid cerasomes and their application in the release of 10-hydroxycamptothecin. *RSC Adv.* **2016**, *6*, 16292–16300. [CrossRef]
42. Markhulia, J.; Kekutia, S.; Mitskevich, N.; Mikelashvili, V.; Saneblidze, L.; Leladze, N.; Jabua, Z.; Sacarescu, L.; Kriechbaum, M.; Almásy, L. Synthesis and in vivo investigation of therapeutic effect of magnetite nanofluids in mouse prostate cancer model. *Dig. J. Nanomater. Biostruct.* **2018**, *13*, 1081–1090.
43. Qiao, Y.; Tahara, K.; Zhang, Q.; Song, X.M.; Kikuchi, J.I. Cerasomes: Soft Interface for Redox Enzyme Electrochemical Signal Transmission. *Chem.—A Eur. J.* **2016**, *22*, 1340–1348. [CrossRef] [PubMed]
44. Claesson, M.; Frost, R.; Svedhem, S.; Andersson, M. Pore spanning lipid bilayers on mesoporous silica having varying pore size. *Langmuir* **2011**, *27*, 8974–8982. [CrossRef] [PubMed]
45. Queisser, H.J.; Michl, J.; Jadhav, P.; Baldo, M.A.; Reilly, T.H.; Kanarr, A.C.; Mohanty, A.; Sussman, J.; Lee, J.; Baldo, M.A.; et al. Multicompartment Mesoporous Silica Nanoparticles with Branched Shapes: An Epitaxial Growth Mechanism. *Science* **2013**, *340*, 337–342. [CrossRef]
46. Alberius, P.C.A.; Frindell, K.L.; Hayward, R.C.; Kramer, E.J.; Stucky, G.D.; Chmelka, B.F. General predictive syntheses of cubic, hexagonal, and lamellar silica and titania mesostructured thin films. *Chem. Mater.* **2002**, *14*, 3284–3294. [CrossRef]
47. Shimojima, A.; Kuroda, K. Designed synthesis of nanostructured siloxane-organic hybrids from amphiphilic silicon-based precursors. *Chem. Rec.* **2006**, *6*, 53–63. [CrossRef]

48. Shimojima, A.; Liu, Z.; Ohsuna, T.; Terasaki, O.; Kuroda, K. Self-assembly of designed oligomeric siloxanes with alkyl chains into silica-based hybrid mesostructures. *J. Am. Chem. Soc.* **2005**, *127*, 14108–14116. [CrossRef]
49. Shimojima, A.; Kuroda, K. Direct formation of mesostructured silica-based hybrids from novel siloxane oligomers with long alkyl chains. *Angew. Chem. Int. Ed.* **2003**, *42*, 4057–4060. [CrossRef]
50. Nunes, S.C.; Toquer, G.; Cardoso, M.A.; Mayoral, A.; Ferreira, R.A.S.; Carlos, L.D.; Ferreira, P.; Almeida, P.; Cattoën, X.; Wong Chi Man, M.; et al. Structuring of Alkyl-Triazole Bridged Silsesquioxanes. *ChemistrySelect* **2017**, *2*, 432–442. [CrossRef]
51. Suzuki, J.; Shimojima, A.; Fujimoto, Y.; Kuroda, K. Stable silanetriols that contain tert-alkoxy groups: Versatile precursors of siloxane-based nanomaterials. *Chem.—A Eur. J.* **2008**, *14*, 973–980. [CrossRef]
52. Besnard, R.; Arrachart, G.; Cambedouzou, J.; Pellet-Rostaing, S. Structural study of hybrid silica bilayers from "bola-amphiphile" organosilane precursors: Catalytic and thermal effects. *RSC Adv.* **2015**, *5*, 57521–57531. [CrossRef]
53. Katagiri, K.; Hashizume, M.; Ariga, K.; Terashima, T.; Kikuchi, J.I. Preparation and characterization of a novel organic-inorganic nanohybrid "cerasome" formed with a liposomal membrane and silicate surface. *Chem.—A Eur. J.* **2007**, *13*, 5272–5281. [CrossRef] [PubMed]
54. Carlos, L.D.; De Zea Bermudez, V.; Amaral, V.S.; Nunes, S.C.; Silva, N.J.O.; Sá Ferreira, R.A.; Rocha, J.; Santilli, C.V.; Ostrovskii, D. Nanoscopic photoluminescence memory as a fingerprint of complexity in self-assembled alkyl/siloxane hybrids. *Adv. Mater.* **2007**, *19*, 341–348. [CrossRef]
55. Nunes, S.C.; Hümmer, J.; Freitas, V.T.; Ferreira, R.A.S.; Carlos, L.D.; Almeida, P.; De Zea Bermudez, V. Di-amidosils with tunable structure, morphology and emission quantum yield: The role of hydrogen bonding. *J. Mater. Chem. C* **2015**, *3*, 6844–6861. [CrossRef]
56. Nunes, S.C.; de Zea Bermudez, V. Structuring of Amide Cross-Linked Non-Bridged and Bridged Alkyl-Based Silsesquioxanes. *Chem. Rec.* **2018**, *18*, 724–736. [CrossRef] [PubMed]
57. Pereira, R.F.P.; Nunes, S.C.; Toquer, G.; Cardoso, M.A.; Valente, A.J.M.; Ferro, M.C.; Silva, M.M.; Carlos, L.D.; Ferreira, R.A.S.; de Zea Bermudez, V. Novel Highly Luminescent Amine-Functionalized Bridged Silsesquioxanes. *Front. Chem.* **2018**, *5*, 131. [CrossRef]
58. Gonçalves, M.C.; Pereira, R.F.P.; Ferreira, P.; Carbó-Argibay, E.; Catita, J.; Toquer, G.; Nunes, S.C.; De Zea Bermudez, V. Structuring of di-alkyl-urethanesils. *J. Sol-Gel Sci. Technol.* **2019**, *89*, 205–215. [CrossRef]
59. Nunes, S.C.; Ferreira, C.B.; Ferreira, R.A.S.; Carlos, L.D.; Ferro, M.C.; Mano, J.F.; Almeida, P.; De Zea Bermudez, V. Fractality and metastability of a complex amide cross-linked dipodal alkyl/siloxane hybrid. *RSC Adv.* **2014**, *4*, 59664–59675. [CrossRef]
60. Nagarajan, R. Molecular packing parameter and surfactant self-assembly: The neglected role of the surfactant tail. *Langmuir* **2002**, *18*, 31–38. [CrossRef]
61. Sagnella, S.M.; Conn, C.E.; Krodkiewska, I.; Drummond, C.J. Nonionic diethanolamide amphiphiles with unsaturated C18 hydrocarbon chains: Thermotropic and lyotropic liquid crystalline phase behavior. *Phys. Chem. Chem. Phys.* **2011**, *13*, 13370–13381. [CrossRef]
62. Angelova, A.; Angelov, B.; Mutafchieva, R.; Garamus, V.M.; Lesieur, S.; Funari, S.S.; Willumeit, R.; Couvreur, P. Swelling of a Sponge Lipid Phase via Incorporation of a Nonionic Amphiphile: SANS and SAXS Studies BT. In *Trends in Colloid and Interface Science XXIV*; Starov, V., Procházka, K., Eds.; Springer: Berlin/Heidelberg, Germany, 2011; pp. 1–6.
63. Milner, S.T.; Safran, S.A.; Andelman, D.; Cates, M.E.; Roux, D. Correlations and structure factor of bicontinuous microemulsions. *J. Phys.* **1988**, *49*, 1065–1075. [CrossRef]
64. Porte, G.; Marignan, J.; Bassereau, P.; May, R. Shape transformations of the aggregates in dilute surfactant solutions: A small-angle neutron scattering study. *J. Phys.* **1988**, *49*, 511–519. [CrossRef]
65. Boyd, B.J.; Rizwan, S.B.; Dong, Y.D.; Hook, S.; Rades, T. Self-assembled geometric liquid-crystalline nanoparticles imaged in three dimensions: Hexosomes are not necessarily flat hexagonal prisms. *Langmuir* **2007**, *23*, 12461–12464. [CrossRef] [PubMed]
66. Berktas, I.; Ghafar, A.N.; Fontana, P.; Caputcu, A.; Menceloglu, Y.; Okan, B.S. Facile synthesis of graphene from waste tire/silica hybrid additives and optimization study for the fabrication of thermally enhanced cement grouts. *Molecules* **2020**, *25*, 886. [CrossRef]
67. Issa, A.A.; Luyt, A.S. Kinetics of alkoxysilanes and organoalkoxysilanes polymerization: A review. *Polymers* **2019**, *11*, 537. [CrossRef]
68. Israelachvili, J.N.; Mitchell, D.J.; Ninham, B.W. Theory of self-assembly of hydrocarbon amphiphiles into micelles and bilayers. *J. Chem. Soc. Faraday Trans. 2 Mol. Chem. Phys.* **1976**, *72*, 1525–1568. [CrossRef]
69. Van'T Hag, L.; Gras, S.L.; Conn, C.E.; Drummond, C.J. Lyotropic liquid crystal engineering moving beyond binary compositional space-ordered nanostructured amphiphile self-assembly materials by design. *Chem. Soc. Rev.* **2017**, *46*, 2705–2731. [CrossRef]
70. Besnard, R.; Arrachart, G.; Cambedouzou, J.; Pellet-Rostaing, S. Tuning the nanostructure of highly functionalized silica using amphiphilic organosilanes: Curvature agent effects. *Langmuir* **2016**, *32*, 4624–4634. [CrossRef]
71. Kaneko, Y.; Iyi, N.; Kurashima, K.; Matsumoto, T. Hexagonal-Structured Polysiloxane Material Prepared by Sol-Gel Reaction of Aminoalkyltrialkoxysilane without Using Surfactants. *Chem. Mater.* **2004**, *16*, 3417–3423. [CrossRef]
72. Qiu, H.; Caffrey, M. The phase diagram of the monoolein/water system: Metastability and equilibrium aspects. *Biomaterials* **2000**, *21*, 223–234. [CrossRef]